INSTITUTE OF PHYSICS PUBLISHING PHYSICS IN MEDICINE AND BIOLOGY

Phys. Med. Biol. **46** (2001) 1245–1264 www.iop.org/Journals/pb PII: S0031-9155(01)18360-0

Mechanical haemolysis in shock wave lithotripsy (SWL): II. *In vitro* cell lysis due to shear

Murtuza Lokhandwalla[1,3], James A McAteer[2], James C Williams Jr[2] and Bradford Sturtevant[1]

[1] Graduate Aeronautical Laboratories, California Institute of Technology, Pasadena, CA, USA
[2] Department of Anatomy and Cell Biology, Indiana University School of Medicine, Indianapolis, IN, USA

E-mail: murtuza@galcit.clatech.edu

Received 26 October 2000, in final form 5 January 2001

Abstract

In this work we report injury to isolated red blood cells (RBCs) due to focused shock waves in a cavitation-free environment. The lithotripter-generated shock wave was refocused by a parabolic reflector. This refocused wave field had a tighter focus (smaller beam width and a higher amplitude) than the lithotripter wave field, as characterized by a membrane hydrophone.

Cavitation was eliminated by applying overpressure to the fluid. A novel passive cavitation detector (HP-PCD) operating at high overpressure (up to 7 MPa) was used to measure acoustic emission due to bubble activity. The typical 'double-bang' emission measured in the lithotripter free-field was replaced by a continuum of weak signals when the fluid was enclosed in a pressure chamber. No acoustic emissions were measured above an overpressure of 5.5 MPa. Aluminium foils were used to study shock wave damage and had distinct deformation features corresponding to exposure conditions, i.e. pitting and denting accompanied by wrinkling. Pitting was eliminated by high overpressure and so was due to cavitation bubble collapse, whereas denting and wrinkling were caused by the reflected shock wave refocused by the parabolic reflector.

RBCs suspended in phosphate-buffered saline (PBS) were exposed to the reflected wave field from a parabolic reflector and also from a flat reflector. Exposure to the wave field from the parabolic reflector increased haemolysis four-fold compared with untreated controls and was twice that of cell lysis with the flat reflector. Recently we analysed deformation and rupture of RBCs when subjected to a flow field set up by a focused shock. The cell lysis results presented here are in qualitative agreement with our theoretical prediction that haemolysis is directly related to the gradient of shock strength and validates shearing as a cell lysis mechanism in SWL.

[3] Present address: General Electric CRD, 1 Research Circle, Niskayuna, NY 12309, USA.

0031-9155/01/041245+20$30.00

1. Introduction

Injury to the kidney in shock wave lithotripsy (SWL) is well documented (Kaude *et al* 1985, Evan and McAteer 1996) and includes damage at the cellular and tissue levels. This damage involves moderate to severe haemorrhage and progression to scarring that can lead to permanent loss of functional renal mass. The physical mechanisms responsible for shock wave injury have yet to be determined. This research was undertaken to explore the idea that shearing due to shock-strength gradient may contribute to shock wave damage in SWL.

Isolated red blood cells (RBCs) have proven to be a sensitive model for studying mechanisms of cellular-level damage due to SWL shock waves (Delius 1997, Stonehill *et al* 1998). Work with cells in suspension has strongly implicated transient acoustic cavitation as a mechanism of shock wave-induced cell lysis (Delius 1997, Stonehill *et al* 1998). Although the correlation between occurrence of cavitation events and cell damage has been fairly strong it has been shown in *in vitro* studies that there is significant cell lysis in absence of cavitation (Williams *et al* 1999b). Experiments with nitrocellulose film (Howard and Sturtevant 1997) immersed in castor oil (a low-cavitation medium), indicated a similar damage pattern. These observations implicate the shock-induced flow field (i.e. shear) as a cause for damage.

Despite the fact that the amount of cell lysis due to this non-cavitational damage mechanism is only a fraction of the damage induced when cavitation is the dominant mechanism, there are several reasons for studying this mechanism, one of the important reasons being that *in vivo* cavitation is highly constrained due to the surrounding tissue and hence less damaging. Experiments simulating this effect (e.g. Zhong *et al* 1999) clearly indicate that bubble growth is significantly reduced when enclosed in a constrained environment. Since most *in vitro* cell lysis experiments are devoid of such *in vivo* constraining effects, cavitation-induced damage is predominant *in vitro* and this may not be true for the *in vivo* environment.

Shock waves propagating in a medium which has randomly distributed acoustic inhomogeneities will cause the shock wave to be attenuated with an increase in rise time. However, a more regular tissue structure such as that present in the kidney cortex and the medulla will result in local focusing/defocusing of the wavefront (see Sturtevant (1996) for a discussion). A focused wave induces a differential tissue motion, commonly referred to as the 'shearing effect'. That haemolysis occurs due to a fluid shearing motion has been amply demonstrated in several experimental configurations, e.g. microstreaming motion near a single resonant bubble (Rooney 1970, 1972, Dunn 1985), or in Couette flow viscometers (Leverett *et al* 1972). A similar shearing effect due to shock wave focusing in SWL may also cause cell lysis provided that the shearing motion is sufficiently strong. To test this idea we enhanced the shearing effect of the SWL shock wave and observed a substantial increase in cell lysis.

In a companion paper (Lokhandwalla and Sturtevant 2001), denoted as paper I in this work, we analysed deformation of RBCs subjected to shock-induced shear flow and bubble-induced radial flow fields. Only extensional fluid motion, induced by the above flow fields, causes the RBCs to deform and induces a tension in the cell membrane. The fluid dynamic forces exerted by the extensional motion are related to the fluid properties (ρ, ν), the cell dimension (r_c), and most importantly to the strength of the extensional flow characterized by a parameter $k(t)$, where t is time. A flow field is lytically effective if membrane tension exceeds a threshold (T_c) and causes the membrane strain to exceed a critical value $(\Delta A/A)_c$. Figure 1 summarizes this perspective of cell deformation/lysis from paper I.

Experiments on RBCs indicate a critical membrane tension, T_c, of 10 mN m^{-1} (1 mN m^{-1} = 1 dyne cm^{-1}), and a $(\Delta A/A)_c$ of 2–3% in order to rupture the cell membrane and cause lysis (Evans *et al* 1976). Calculations in paper I indicate that the lithotripter-generated shock induces a shear flow which can exert a tension of $\sim$100 mN m^{-1} on the membrane.

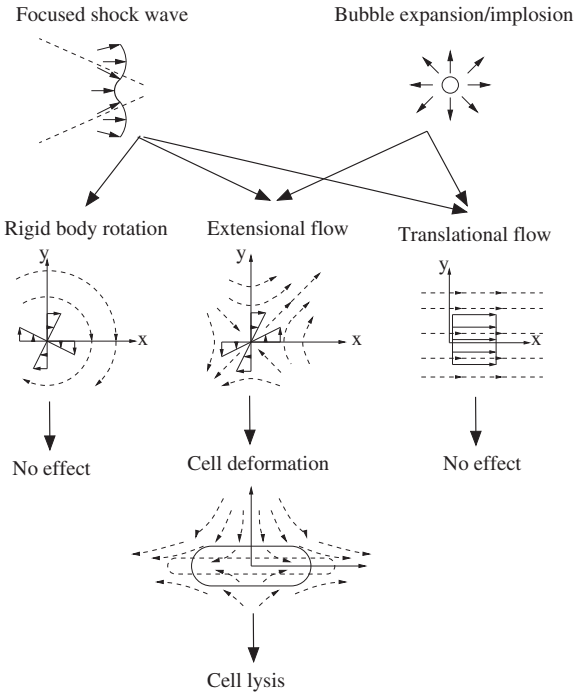

Figure 1. Cell deformation/lysis induced by fluid motion. Full arrows are velocity profiles and broken arrows are streamlines for each flow-field.

However, the membrane strain is exceedingly small, $(\Delta A/A) \sim 10^{-5}$, which explains the very small fraction of lysed cells (Williams *et al* 1999b) due to lithotripter shock-induced shear. Thus, by changing these parameters (i.e. ρ, ν, r_c, $k(t)$, T_c), membrane deformation can be altered leading to a commensurate change in cell lysis. In this work the flow field was modified (i.e. the parameter $k(t)$ was enhanced), resulting in an increased cell lysis.

For a two-dimensional flow field, for instance, the relation between the extensional flow parameter ($k(t)$) and the flow field ($\vec{u}^{\infty}(x, y)$) is given by $\vec{u}^{\infty}(x, y) = (k(t)x, -k(t)y)$, where (x, y) are spatial coordinates in Cartesian system. If the shockfront is assumed to be planar, with maximum strength at the acoustic axis of the lithotripter and decaying off-axis, then $k(t)$ is the gradient of the particle velocity along the wavefront, given by $k(t) = \partial u_z/\partial r$, where z is the direction of propagation of the wavefront (acoustic axis) and r is measured along the wavefront. For a curved shockfront of uniform strength, with a radius of curvature R and fluid particle velocity u_R, the parameter $k(t)$ is given by u_R/R. Both these effects, wave gradient and wave curvature, contribute to the parameter $k(t)$. Thus, a tighter focus with a smaller beam width (and consequently a higher shock-strength gradient) and smaller wavefront curvature results in an increased $k(t)$.

The localized focusing effect of *in vivo* acoustic inhomogeneities results in an increased wave gradient. *In vitro* an acoustically heterogeneous medium such as a suspension of polystyrene spheres in agar can provide a similar 'lens' effect. However, such a medium also attenuates the shock wave and negates the focusing effect. Suspending RBCs in such a medium would be a difficult task. Since a reflector can also focus a shock wave it will have a 'lens' effect similar to that of an acoustically heterogeneous medium. Such a reflector has advantages over a heterogeneous medium, in that it is easier to construct and there is no

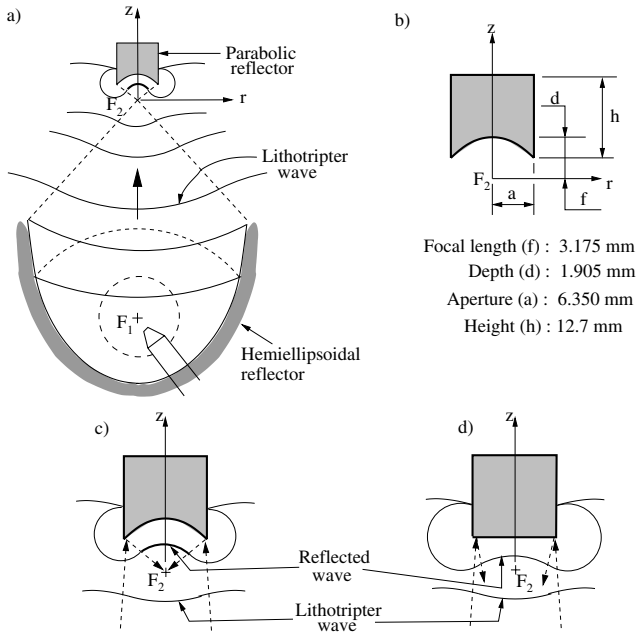

Figure 2. Schematics of shock wave reflectors. (*a*) Arrangement of the hemiellipsoidal reflector of the lithotripter and the parabolic reflector positioned confocally with F2. The broken circle represents the spherical wavefront generated at the spark gap. Full lines indicate the shock wave reflected off the hemiellipsoidal reflector (see Sturtevant (1996) for a discussion on shock wave focusing in lithotripters). (*b*) Dimensions of the parabolic reflector. (*c*), (*d*) Geometry of waves reflected off the parabolic (*c*) and flat (*d*) reflectors. Broken arrows indicate rays while full lines are wavefronts.

attenuation of the shock wave. However, with a reflector there will be waves diffracted from its edge that would be absent from the wave field of a heterogeneous medium. A parabolic reflector was used in this work to refocus the lithotripter shock wave and thereby simulate the focusing effect of an acoustically heterogeneous medium.

The parabolic reflector was positioned confocally with the external focus (F2) of the hemiellipsoidal reflector of the lithotripter. Figure 2(a) shows a schematic of the reflector configuration. A similar reflector arrangement has been reported by Eisenmenger *et al* (1997). Cavitation was controlled by applying overpressure to the region surrounding F2 (Williams *et al* 1999b, Stonehill *et al* 1998). The overpressure above which cavitation activity was inhibited was determined by a novel cavitation detector which operates at high overpressure (HP-PCD). Thus, our experimental set-up enabled us to enhance the shock wave focusing effect, monitor acoustic emissions and apply overpressure to suppress cavitation. Aluminium foils were also used to evaluate damage patterns due to exposure to the lithotripter wave field and the refocused wave field.

Research lithotripters constructed at the Graduate Aeronautical Laboratory, California Institute of Technology (GALCIT) were used for these experiments (see Cleveland *et al* 2000b). Cell lysis and foil damage experiments were conducted at Indiana University School of Medicine (IU) while other measurements were done at GALCIT. The research lithotripters used at GALCIT and IU have identical electrical and mechanical parameters, and have been designed to mimic the Dornier HM3. A detailed comparison of GALCIT, IU and Dornier HM3 lithotripters, describing their acoustic fields and electrical/mechanical parameters, has

been reported elsewhere (Cleveland *et al* 2000b). The experimental set-up at IU for exposing a cell suspension to shocks under a controlled overpressure was reported earlier (Stonehill *et al* 1998). Cells were subjected to the wave field refocused by a parabolic reflector. A flat reflector was used as a control. The reflectors used at both the laboratories had identical dimensions. This enabled us to compare cell lysis results from experiments at IU with acoustic measurements made at GALCIT, under similar conditions.

2. Materials and methods

2.1. Acoustic fields

In this text the lithotripter-generated wave field which is incident on a parabolic or flat reflector is called the 'lithotripter wave field'. The term 'reflected wave field', is used to identify the result of the reflection of the lithotripter wave field off the above reflectors. The term 'refocused wave field' will be used occasionally as a synonym for reflected wave field in reference to the refocusing effect of the parabolic reflector.

2.1.1. Lithotripter wave field. In an electrohydraulic lithotripter a pressure pulse is generated by a spark gap located at the internal focus (F1) of a hemiellipsoidal reflector. In the case of the research lithotripters used in these studies, the hemiellipsoidal reflector sits at the bottom of a water tank filled with a weak electrolyte ($NaHCO_3$ or NaCl solution, 660 μS cm^{-1} conductivity). Storage capacitors apply a high voltage across the spark gap forming a conducting plasma channel that vaporizes the electrolyte. This vapour bubble expands rapidly generating a spherical wavefront centred at F1. A sector of this spherical wavefront is focused to the external focal point (F2) of the hemiellipsoidal reflector (figure 2(*a*)). A characteristic feature of this spark gap and ellipsoidal reflector system is that small changes in source geometry cause large aberrations at F2.

2.1.2. Reflected wave field. The parabolic reflector was oriented such that its focus coincided with the F2 focal point of the hemiellipsoidal reflector (figure 2(*c*)). The reflector surface was a paraboloid of revolution. Dimensions (figure 2(*b*)) were chosen so that the reflector would fit into the vials used to hold RBCs and still maximize the portion of the lithotripter wave that would be reflected. Since the lithotripter shock wave in the vicinity of F2 is not perfectly planar, the wave reflected off the parabolic reflector is focused to a point just proximal to the geometric focal point of the paraboloid (figure 2(*c*)). Shear should be greatest in this region. The flat reflector was, likewise, aligned coaxially with the symmetry axis of the hemiellipsoidal reflector with the reflecting surface 4 mm above F2. The overall dimensions of the flat reflector (a and h in figure 2(*b*)) were identical to that of the parabolic reflector.

The focusing effect of the parabolic reflector is applicable in the limit of geometrical acoustics; that is, incident waves of the lithotripter wave field of wavelength λ much smaller than a characteristic reflector dimension (f or a in figure 2(*b*)) will be focused. Since the lithotripter wave has a range of frequency components (the shockfront is estimated to be 60 nm thick for a shock strength corresponding to 35 MPa—see Sturtevant (1996)—whereas overall pulse length is about 8 mm), only the high-frequency components ($\lambda \ll 3$ mm) get focused while the remainder is scattered by the reflector. Similar shock-focusing reflectors have been used in gas-filled shock tubes (Sturtevant and Kulkarny 1976) where plane shocks of various strengths were focused by parabolic reflectors. There is one important difference, however, between the shock tube experiment and the present case. In SWL the shockfront

decays in $\sim$2 μs (3 mm) which is comparable to reflector dimensions, whereas the above-mentioned experiments had a constant shock strength for a length scale much larger than any reflector dimension.

The pressure traces reported here were measured using a commercial polyvinylidene fluoride (PVDF) membrane hydrophone (model 301, Sonic Industries, Hatsboro, PA), which utilizes the piezoelectric effect of PVDF. The sensitive element of the hydrophone had a nominal diameter of 0.5 mm and a flat response up to 50 MHz (as per the manufacturer). Other details of this hydrophone and the supporting apparatus, have been reported elsewhere (Cleveland *et al* 2000b). All waveform measurements reported in section 3.1 were performed with a lithotripter setting of 18 kV and subsequent shots were fired at intervals of greater than 15 s. Conditioning of the water used in the lithotripter test tank and for immersing the hydrophone was identical to that used by Cleveland *et al* (2000b).

2.2. Bubble dynamics

The response of a single bubble in an unbounded fluid subjected to a typical lithotripter pulse (a positive shockfront followed by a negative tail) has been studied in detail (Church 1989, Choi *et al* 1993). The leading positive pressure of the wavefront causes the bubble to collapse. This initial collapse is accompanied by a corresponding acoustic emission. Subsequently the trailing negative pressure in the pulse causes the bubble to grow rapidly. The inertia of the surrounding fluid causes this bubble to keep growing to several times its initial size, even after the lithotripter pulse has propagated past the bubble. As the bubble grows the pressure inside falls to much lower than the initial equilibrium pressure. This stops bubble growth. At this point the bubble is essentially a 'void' as it has expanded to several times its original size. The surrounding fluid now rushes inward and causes the void to collapse. This is referred to as either 'Rayleigh collapse' or 'inertial collapse' since collapse is driven by the inertia of the surrounding fluid. Inertial collapse is also accompanied by an acoustic emission that is calculated to be much stronger than the original collapse (Church 1989). Hence cavitation bubble activity in lithotripsy can be characterized by the occurrence of two prominent acoustic emissions (i.e. 'double-bang') detected by a hydrophone.

Theoretical studies of cavitation bubble dynamics address the behaviour of solitary bubbles. However, experiments using high-speed photography have amply demonstrated a bubble cloud in the vicinity of F2 (Saas *et al* 1991, Zhong *et al* 1997). Although the above description of bubble growth and collapse would still apply qualitatively to individual bubbles in the cloud, we expect cloud dynamics to play an important role in determining bubble response. Thus, we expect discrepancies between analytical single-bubble model predictions and *in vitro* emission measurements.

In this section we detail our cavitation detection system used for measuring bubble emission under conditions of altered ambient pressure. A passive cavitation detector (PCD), similar to that used by others (Cleveland *et al* 2000a, Coleman *et al* 1992, Zhong *et al* 1997), was used to measure acoustic emissions from bubble activity in the focal region of the lithotripter. Typically, a PCD consists of a focused piezoceramic receiver designed such that it detects acoustic emissions from cavitation activity occurring in the focal region of the receiver. It is also intended that the PCD affects bubble dynamics only minimally, hence the name 'passive'. An important design feature of the PCD used in our work is that it was coupled with a pressure chamber. This allowed us to increase the overpressure of the fluid in the vicinity of F2 and simultaneously to measure the acoustic emission due to bubble activity.

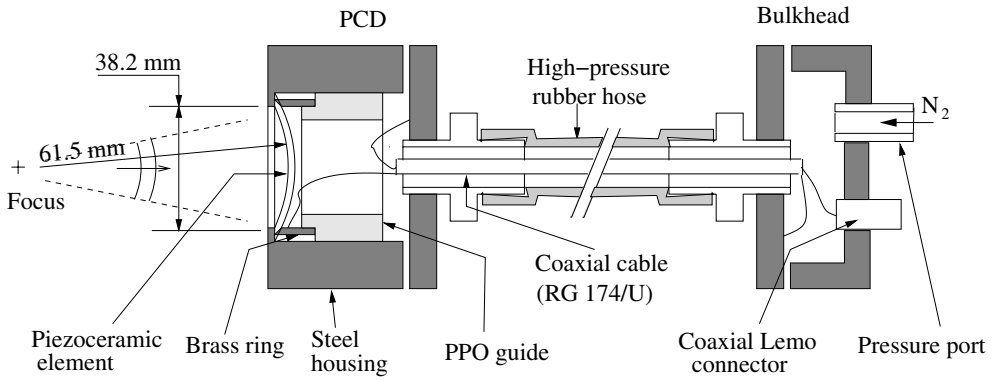

Figure 3. Schematic of the PCD and the bulkhead.

2.2.1. PCD. The PCD piezoceramic element was a spherical segment (i.e. bowl) 2 mm (0.08″) thick, 61.5 mm (2.42″) radius of curvature, and an aperture diameter of 38.2 mm. The element was made of lead zirconate titanate (Channel Industries Inc., Santa Barbara, CA; C 5400) with a silver coating on its two faces which served as electrodes. It had a resonant frequency of 1 MHz in the thickness mode and 54 kHz in the planar/radial mode (i.e. the mode in which radial dimension of the element changes). The bowl was held in a stainless-steel water-tight housing designed to sustain 7 MPa (≈1000 psi). The element was held in place by a brass ring. The assembled configuration of the housing, the element and the brass ring is illustrated in figure 3. The brass ring was electrically isolated from the housing by a cylindrical guide made of polyphenylene oxide (PPO) (McMaster Carr, Los Angeles, CA; 8561K351). Conductive O-rings (Tecknit, Cranford, NJ; 87-10512) were used between the element faces, the housing and the brass ring (not shown in figure).

The cover of the PCD housing had a port to which was connected a high-pressure rubber hose (Swagelok Co., Solon, OH; SS7R4-PM4-PM4-24). A coaxial cable (RG 174/U, 50 Ω impedance, 0.11″ (2.8 mm) nominal diameter) and compressed nitrogen (N_2) both entered the PCD housing through the high-pressure hose. The high-pressure hose was connected to a bulkhead located outside the lithotripter test tank. At the bulkhead the coaxial cable and the N_2 supply were separated. A high-pressure coaxial connector (LemoUSA, Santa Rosa, CA; 0E series coaxial plug and receptacle) was used to lead the signal out of the bulkhead. The bulkhead was connected to a manifold which supplied N_2 at regulated pressure. This design allowed us to make a water-tight electrical connection to the pressurized PCD housing. The transducer could either be air-backed or the housing could be filled with oil (or any other non-conducting fluid). Experiments were performed either with air or oil as the backing and there was no significant difference in the results. Results reported here are with an air-backed transducer only.

The acoustic field of the focused receiver was characterized using a PVDF needlephone (Imotec Messtechnik, Warendorf; type 80-0.5-4.0). The needlephone had a sensitive diameter of 0.5 mm and could resolve a rise time of 50 ns. Gated sinusoidal waves of 1 MHz, 20 V peak-to-peak amplitude produced by a function generator (Hewlett-Packard, Palo Alto, CA; 33120A) were applied to the focused receiver and the acoustic field was scanned by the needlephone. The waves were 10 cycles long, sufficient to achieve a steady acoustic field without causing reverberations from the lithotripter test tank. The acoustic field attained a maximum at the focus of the receiver. Typically, focused transducers are characterized by the dimensions of a cylindrical 6 dB region near the focus. For our PCD this region was measured to have a

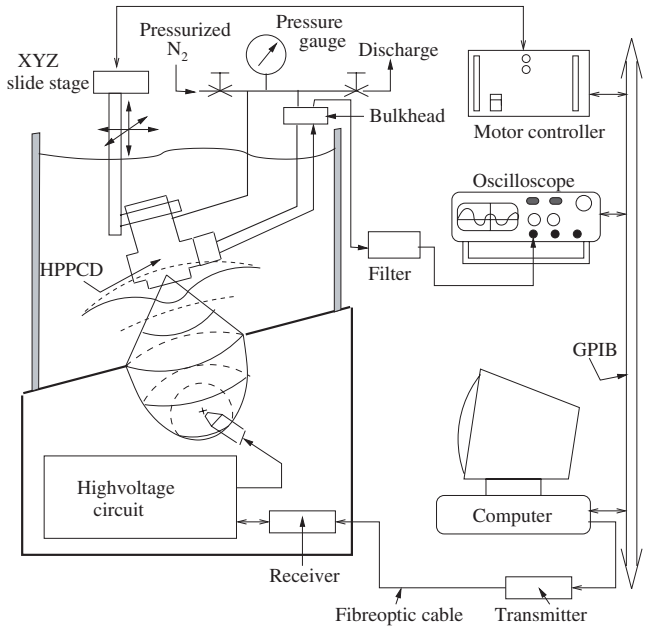

Figure 4. Overview of the experimental set-up, depicting the lithotripter, the computer, the HP-PCD and other accessories. Thick full lines are high pressure supply lines for N_2. See text for details.

diameter of 3.7 mm and a length of 36 mm and compared well with the transducer parameters of other investigators (see Cleveland *et al* (2000a) for comparison). The dimensions of the 6 dB region of the focused hydrophone was also calculated using O'Neil's approximation (O'Neil 1949), and found to be 3.3 mm and 35.8 mm respectively.

Since only the thickness mode signal (1 MHz) is related to bubble activity the low-frequency mode (54 kHz) was filtered out with a combination of passive and active filters. The passive filter was a simple RC high-pass circuit with a 3 dB cut-off point at 300 kHz ($R = 1\,\mathrm{k}\Omega$, $C = 530$ pF). The passive filter reduced the radial mode and thickness mode signals to one-third and 85% of their respective original amplitudes. This signal was further processed by an active filter (Krohn-hite, Avon, MA; model 3202) set at a high-pass of 800 kHz. A test signal combination of the two modes (1 MHz, 54 kHz) was produced by the function generator to test the performance of the combined filter. The lower-frequency mode was reduced to less than 5% of the thickness mode signal. In the thickness mode the piezoceramic element had a sensitivity of 53.1 V MPa^{-1} (sensitivity = voltage/pressure = $g_{33}t$, where $g_{33} = 0.0261$ V m N^{-1} was the piezoelectric constant, as cited in the manufacturer's catalogue, and $t = 2$ mm was the element thickness).

The piezoceramic element combined with the above filter renders it as a narrowband transducer with a resonant frequency of 1 MHz, whereas acoustic emission during inertial collapse of a bubble is reported to be a broadband pulse of very short duration ($\ll 1\ \mu$s) (see Vogel and Lauterborn 1988). Evidently the PCD could not resolve any temporal features of this acoustic emission. A broadband transducer like the membrane hydrophone or the needlephone could resolve more temporal variations but these did not have sufficient sensitivity to detect these emissions. Corresponding to each bubble emission impinging on the piezoceramic element, the output is an exponentially decaying sinusoid of 1 MHz frequency. Although it is possible to extract the energy of the acoustic impulse from this signal (see Cleveland (2000a)

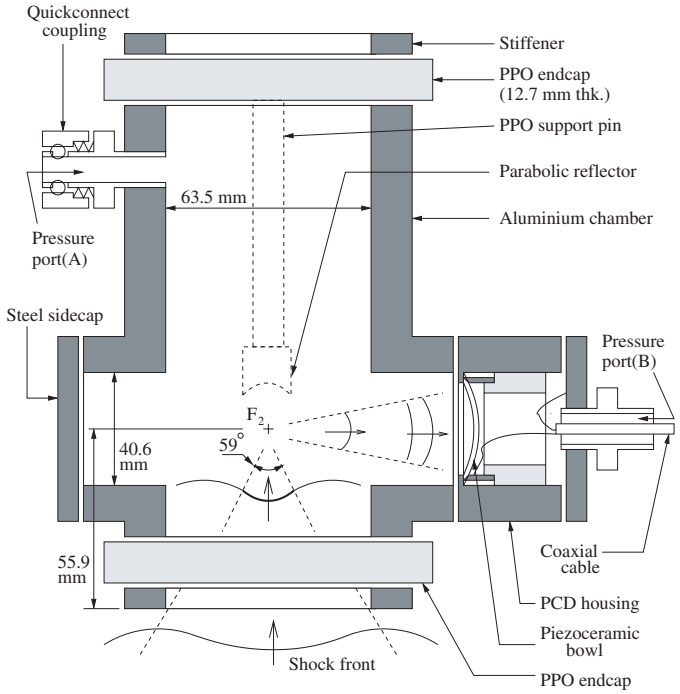

Figure 5. Pressure chamber and the PCD (HP-PCD) set-up, used for measuring cavitation emission, at static pressures higher than ambient. See section 2.2.2 of the text for details.

for details) the electrical output is presented (section 3.2) without any further processing. These traces (section 3.2) clearly show the timing and relative amplitude of cavitation events.

The filtered signal was digitized by an oscilloscope (Tektronix, Inc., Beaverton, OR; TDS 540A) triggered by a Rogowski coil which measured the discharge current at the lithotripter electrode. The oscilloscope was connected to a PC (Pentium 166 MHz) by a general-purpose interface bus (GPIB/IEEE 488.2) through which all communication and data transfer took place. The PC also provided a trigger to a fibre-optic module which in turn triggered the lithotripter (see Cleveland *et al* (2000b) for details). Acoustic emissions were measured for single shocks (minimum time interval of 15 s between consecutive shocks) at a lithotripter setting of 18 kV. A commercial software package (National Instruments, Austin, TX; Labview) was used to automate these tasks (trigger the lithotripter, initialize the oscilloscope to acquire the PCD signal and store the PCD signal on the PC hard-drive). Figure 4 shows a schematic of this entire set-up.

2.2.2. Pressure chamber. The pressure chamber used for the HP-PCD set-up was a hollow aluminium cylinder 63.5 mm (2.5″) internal diameter, 12.7 mm (0.5″) wall thickness and 152.4 mm (6″) long (figure 5). PPO end-caps (12.7 mm (0.5″) thick) were used to cover the cylinder ends. The PPO end-caps have been reported to minimally modify the shock wave (Stonehill *et al* 1998) and at the same time these have sufficient tensile strength to sustain an internal pressure of 10 MPa. The pressure chamber alone could be pressurized to 10 MPa but the HP-PCD could only withstand 7 MPa. Thus, the pressure chamber reported here was similar to that used at IU (Stonehill *et al* 1998) except for the presence of two circular side-windows 40.6 mm in diameter. Cylindrical aluminium flanges were welded to the pressure

chamber to serve as side-windows enabling us to couple the PCD to the pressure chamber. When not in use the side-windows were covered with steel side-caps. Stainless-steel stiffeners were bolted with the PPO end-caps in order to minimize the deflection of end-caps. The side-windows were designed such that the PCD focused on the chamber axis 55.9 mm from the bottom end of the cylinder assembly.

The cylinder had a port (pressure port (A) in figure 5) that could be connected to a high-pressure hose (Swagelok Co., Solon, OH; SS7R4-PM4-PM4-24) using a quick-connect coupling (Swagelok Co., Solon, OH; B-QF-4 series). The other end of this hose was connected to the same N_2 manifold that also supplied the PCD through a pressure port (B). The N_2 manifold connected to a N_2 cylinder. A pressure regulator, control valve, pressure gauge and discharge valve were provided on this manifold (see figure 4). Thus, both the pressure chamber and the PCD were pressurized to the same level. Hence, there was no pressure difference across the piezoceramic element and consequently no tensile stresses associated with the overpressure (with a tensile strength of 76 MPa the 2 mm thick piezoceramic element is able to withstand 1 MPa overpressure applied to one side). Two miniature C-clamps were included within the chamber for holding aluminium foils or polymeric films at F2. A cylindrical PPO support pin was attached to the top PPO end-cap to hold the parabolic or flat reflector. The HP-PCD assembly was mounted on a stepper-motor driven X-Y-Z slide (Velmex-Unislide, East Bloomfield, NY; MB40(12/15)K1J-S4) which enabled us to align the HP-PCD assembly with the lithotripter acoustic axis and F2. The controlling unit for these stepper motors communicated with the PC through the GPIB bus (figure 4).

The internal diameter of the pressure chamber (63.5 mm) and the axial location of F2 from the bottom end of the chamber assembly (55.9 mm) created an effective aperture of 59° (figure 5). The aperture of the hemiellipsoidal reflector of the lithotripter is 68° (Cleveland *et al* 2000b), thus we expect some truncation of the wavefront. This was assessed by measuring the waveform at F2 inside the pressure chamber using the Imotec needlephone. The peak positive and negative pressures of the lithotripter pressure trace were reduced by less than 5% and the overall wave profile was not altered despite the presence of the pressure chamber. With the PCD assembled to the pressure chamber the needlephone was introduced from the opposite window and the acoustic field of the PCD was scanned (procedural details discussed in section 2.2.1). The acoustic field of the PCD was unchanged, indicating that the reflections from the chamber or window walls did not influence the acoustic field of the focused hydrophone.

2.3. Damage to aluminium foils

Aluminium foil (Reynolds Wrap from Reynolds Metals Co., Richmond, VA; 38 μm thick) targets were used to study shock-wave damage. The targets were exposed to the lithotripter wave field and the refocused wave field at different overpressures. The targets were oriented perpendicular to the acoustic axis of the lithotripter. Procedural details for mounting the foils in the pressure chamber were identical to those described previously (Stonehill *et al* 1998). After shock wave exposure, foils were photographed using a digital camera (Nikon; CoolPix 990). Results are discussed in section 3.3 and are for a lithotripter setting of 20 kV at 1 Hz pulse repetition rate.

2.4. Cell lysis

Cell lysis experiments carried out in this study were similar to those described previously (Williams *et al* 1999b) with the exception that the cells were held in a vial stoppered with a parabolic (or flat) reflector. Brass reflectors were used for the acoustic and bubble emission measurements described in sections 2.1 and 2.2 while stainless-steel reflectors were used with

cells. The acoustic impedance of brass is very close to that of stainless steel (27 and 30 times that of water), so the reflectors were considered to be acoustically equivalent. Briefly, freshly drawn human RBCs were washed with phosphate-buffered saline (PBS) and suspended at a volume concentration of 3.1%. Vials fashioned from the bulb end of polyethylene pipettes (Williams *et al* 1999a) were filled with cell suspension and then plugged with a reflector. Care was taken to avoid introducing bubbles into the vial. If bubbles were visible then the vials were discarded. This resulted in a polyethylene container with rounded end filled with the RBC suspension (about 2 ml total) that was in direct contact with the reflector (see figure 12(*a*)).

Studies with RBCs were performed using the overpressure chamber at IU (Stonehill *et al* 1998). Vials were mounted round-end down, centred on the acoustic axis and positioned so that the F2 of the lithotripter (corrected for the focusing effect of PPO) was 3 mm from the aperture plane of the parabolic (or flat) reflector. Prior to shock wave treatment the pressure in the chamber was adjusted to ∼12 MPa. Vials were exposed to 150 shock waves (20 kV, 1 Hz). Controls included vials that were pressurized and not exposed to shock waves, and vials that were not pressurized and not shock wave treated. Following shock wave exposure in the presence of either the parabolic or flat reflector an aliquot of cell suspension was taken for measurement of cell lysis. The cell suspensions were centrifuged at 6000*g* for 10 min and absorbance of the supernatant measured at 414 nm. Cells in the pellets were lysed with detergent and absorbance was similarly determined. Lysis was calculated as the percentage of total haemoglobin released into the supernatant.

3. Results

3.1. Acoustic fields

Figure 6 shows representative waveforms measured by the membrane hydrophone positioned in the plane of F2 at different points lateral to the acoustic axis ($r = 0$). These traces capture both the lithotripter waveform and the waveform reflected off the parabolic (or flat) reflector. The lithotripter pressure trace measured on the acoustic axis ($r = 0$ in figure 6) has a leading positive shockfront which decays to zero in 1–2 μs followed by a negative tail of 4–6 μs duration. The amplitude of the shockfront at F2 (denoted as $p^+_{\max}$), is measured to be ≈35 MPa (see Cleveland *et al* 2000b). Though measurements indicate a shock rise time of 50 ns the shockfront is estimated to be 40 ps (60 nm) thick (see Sturtevant 1996) at this shock strength (35 MPa). The negative tail has an amplitude (p^-) of 10 MPa. The wave amplitudes decay with distance off-axis such that the 6 dB beam-width (location where shock amplitude is half peak value) is ∼10 mm. This is illustrated in figures 7(*a*) and 7(*b*), where the broken curve plots the off-axis distribution of peak pressures (p^+, p^-) for the lithotripter wave. Similar pressure traces and peak pressure distribution for the Dornier HM-3 have been reported in literature (Müller 1990, Coleman 1987a).

Pressure trace and acoustic field measures were collected using the membrane hydrophone positioned immediately in front of (proximal to) the parabolic (or flat) reflector. Thus, the lithotripter wave hits the hydrophone before it strikes the reflector, to be reflected back to hit the hydrophone a second time. The time required for the wave to travel from the hydrophone to the reflector and back is approximately 5 μs. In figure 6 a reflected shock with a 50 ns rise time is clearly seen for the flat reflector (right column). For the parabolic reflector (left column) the reflected shock did not show a similar rise time. This was due to difficulty in aligning the reflector and the hydrophone at F2. Even with perfect alignment of the hydrophone and the parabolic reflector along the acoustic axis and F2, the shot-to-shot variability of the lithotripter rendered this alignment meaningless.

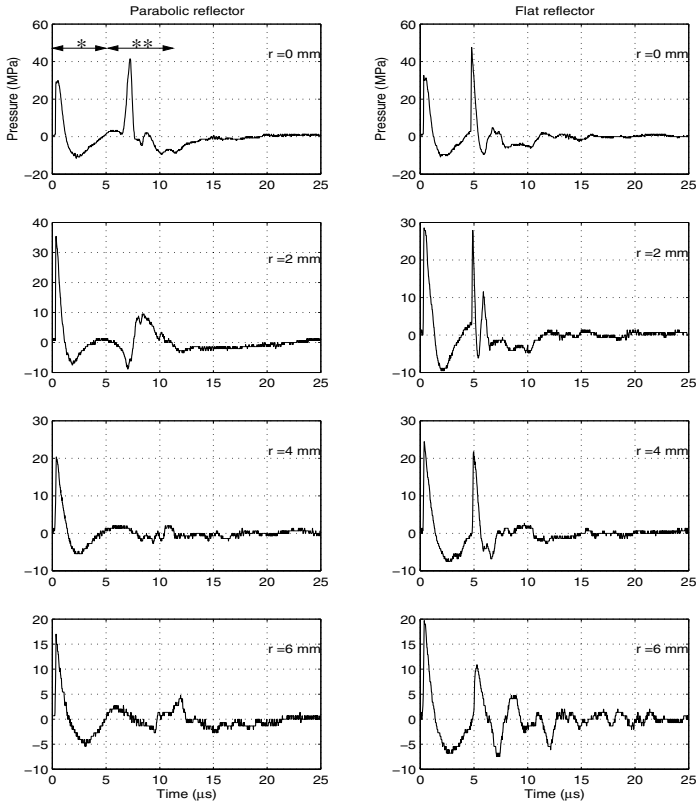

Figure 6. Pressure traces measured in the plane of F2 at $r = 0$, 2, 4 and 6 mm off the acoustic axis ($r = 0$) in the presence of a parabolic (left column) or flat (right column) reflector. The leading pulse (first 5 μs) is the lithotripter wave (*) and the trailing pulse is the reflected wave (**).

Table 1. Comparison of acoustic fields.

	p^+_{max} (MPa)	6 dB width (mm)	k ($\sim \partial u_z/\partial r$) ($s^{-1}$)
Lithotripter wave	35–40	10	1.25×10^3
Reflected wave:			
Parabolic reflector	37	5	2.5×10^3
Flat reflector	38	7	1.8×10^3

The off-axis peak pressure amplitudes (p^+, p^-) for the parabolic and flat reflector wave fields and the lithotripter wave field are shown in figure 7. Table 1 lists the values for p^+_{max}, 6 dB width and the resultant velocity gradient (k). The velocity gradient is calculated from the acoustic velocity due to p^+_{max} and the 6 dB width ($k = 1/2(p^+_{max}/\rho c)/6$ dB width). As expected, the shock wave focusing effect of the parabolic reflector results in a higher value of parameter k (due to a higher p^+_{max} and a smaller 6 dB width) than the original lithotripter wave. The wave reflected off the flat reflector also has some focusing effect. A possible explanation is that the lithotripter wave incident on the reflector may not be perfectly planar, but may have some curvature. The parameter k, which is a measure of the rate of flow-field deformation, and hence its lytic effectiveness, is highest for the wave field reflected off the parabolic reflector.

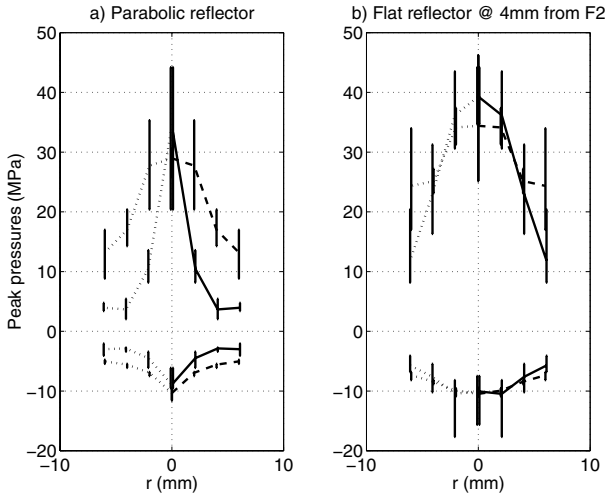

Figure 7. Off-axis peak pressures measured at $r = 0, 2, 4$ and 6 mm from the acoustic axis ($r = 0$). Full and broken curves indicate the reflected and lithotripter wave fields respectively. Scans shown for $r < 0$ are shown dotted, since these are replicas of $r > 0$, flipped over. (*a*) Parabolic reflector. (*b*) Flat reflector.

3.2. Acoustic emission measurements

The acoustic emission measurements described below are divided into two parts: 'free-field' and 'closed-field' measurements. Acoustic emission measurements made using the PCD without any pressure chamber are denoted as free-field, whereas those obtained by the HP-PCD are denoted as closed-field.

3.2.1. Free-field acoustic emission. Figure 8 illustrates representative free-field PCD traces with and without the parabolic (or flat) reflector positioned at the shock wave focus. In all cases the timescale has been offset by the amount of time elapsed from the instant the capacitor discharges (detected by the Rogowski coil) to the instant when the first acoustic emission reaches the piezoceramic element. This total time (228 μs) is a summation of travel time taken by the lithotripter wave to reach F2 (186.6 μs) and for the acoustic emission to travel from F2 to the PCD (41.3 μs). Thus, for all cases, the signal measured at $t \sim 0$ is either an emission resulting from initial bubble collapse (see section 2.2) or the shock wave scattered from bubbles located at F2. In the presence of reflectors the shock wave scattered from the reflectors also contributes to this signal. For the free-field case without any reflector the second emission (i.e. from inertial collapse) occurs at $t \sim 300$ μs, of about 0.5 V amplitude. In the vicinity of the second emission (300 μs) other smaller signals can also be seen. One plausible explanation is that the collapsing bubble regrows and recollapses; that is, it rebounds after the first inertial collapse. Alternatively these signals could be due to cavitation events occurring outside the focal region of the lithotripter (F2). In this case the signal might reach the PCD earlier than the emissions from the region of F2.

For the lithotripter wave the time between the two collapse events was found to vary from 250 to 350 μs (figure 8(*a*)). This is in good agreement with other measurements (from figure 6(*a*) in Cleveland *et al* 2000a, this time is 250–325 μs for identical experimental conditions). The acoustic emissions were also measured transverse to the acoustic axis. The amplitude of the emissions decayed with distance from F2; however, the time between the

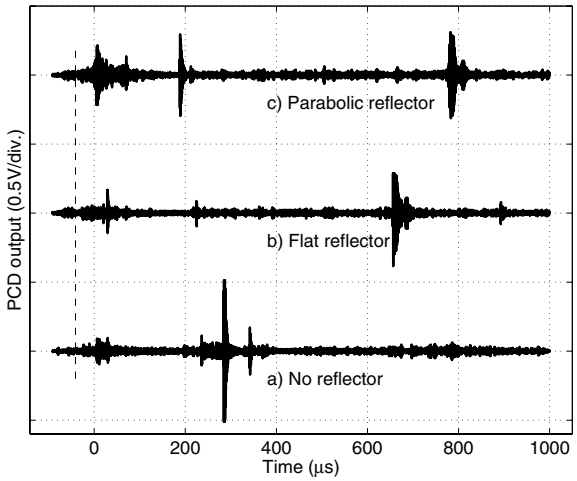

Figure 8. Free-field bubble emission (i.e. no pressure chamber, at ambient pressure) as detected by the PCD. The timescale has been offset by the time taken by bubble emission at F2 to reach PCD. The broken line (at -41.3 μs) indicates the time of the arrival of the shock wave at F2. (*a*) Response to lithotripter wave. (*b*) Flat reflector. (*c*) Parabolic reflector. Measurements are offset by multiples of 1 V for clarity.

two collapses remained in the same range. This observation is consistent with bubble-cloud behaviour rather than the activity of a single bubble which would predict a smaller collapse time owing to the reduced amplitude of negative pressure (p^-) of the lithotripter wave field.

With the reflectors (figures 8(*b*) and 8(*c*)) the weak emission at $t \sim 0$ was followed at $\sim$200 μs by another relatively weak signal (<0.3 V). This was followed at $t \sim$ 600–800 μs by another emission of similar amplitude. It is possible that this third emission is due to cloud collapse and that the timing is delayed because of the presence of the reflector. Single-bubble calculations (using the Rayleigh model (Rayleigh 1917)) with the bubble subjected to a lithotripter wave and reflected wave did not predict such a modification in the timing or strength of the collapse events. This modification was probably due to bubble-cloud dynamics and the presence of the rigid reflector wall close to the bubble cloud. Single-bubble models assume an unbounded fluid, a condition no longer satisfied in this case due to proximity of the reflector to the bubble cloud.

3.2.2. Closed-field acoustic emission. Figure 9 shows measurements of the lithotripter wave field using the HP-PCD with increasing overpressure (0–5.5 MPa). The acoustic emission measured at 0 MPa overpressure was significantly different from that in the free field (figure 8(*a*)) even though the lithotripter wave field was identical (see section 2.2.2). The water used in both these measurements (i.e. free-field and closed-field) was identical and same as that of the lithotripter test tank. In order to fill the pressure chamber with water it was immersed in a water-filled trough and the side-caps and end-caps were assembled under water. The high-pressure hose was also partially filled. This ensured that there were no air bubbles trapped inside the chamber. All other experimental parameters (e.g. firing rate, supply voltage setting, filters used for signal processing) were the same.

Inertial collapse expected at 250–350 μs following the primary collapse was not detected. Instead of exponentially decaying sinusoids which indicate discrete events in the bubble growth–collapse cycle a continuum of weak signals (<0.2 V) was recorded over the 0–500 μs

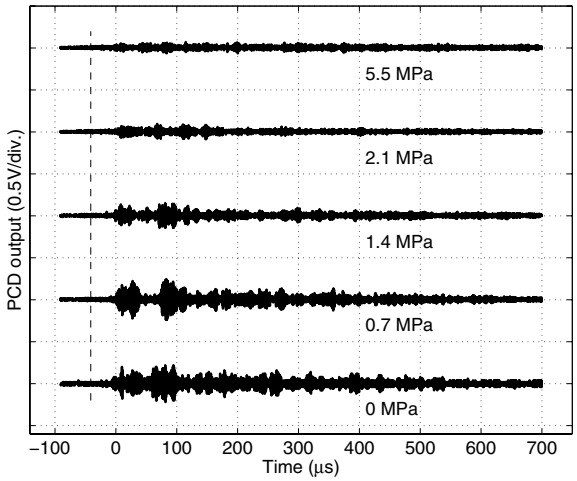

Figure 9. Closed-field bubble emission in response to the lithotripter wave. Shows the effect of increasing overpressure (0–5.5 MPa).

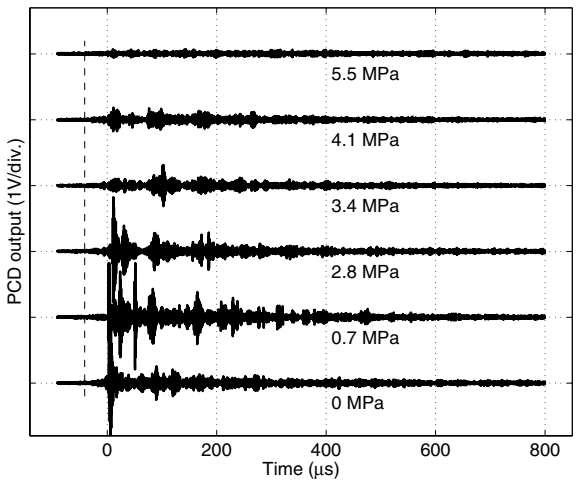

Figure 10. Closed-field bubble emission in response to the wave reflected by the parabolic reflector. Shows the effect of increasing overpressure (0–5.5 MPa).

period. The source of these signals is not clear, but we speculate that the coherent bubble-cloud collapse which was responsible for the typical double-bang signature no longer exists or was too weak to be detected. Increased overpressure caused these signals to diminish in strength and duration until eventually no signals were detected (at 5.5 MPa). Investigating bubble dynamics in this closed-field is beyond the scope of this work, and it suffices to state here that no bubble activity was detected beyond a threshold overpressure of 5.5 MPa.

Figure 10 shows the emission measurements using the HP-PCD for the wave field reflected by the parabolic reflector at increasing overpressure (0–5.5 MPa). Regardless of the overpressure there was no emission seen at either 250–350 μs or at 600–800 μs. However, very strong emissions occurred at $t \sim 0$ which could be due to scattering of the shock wave

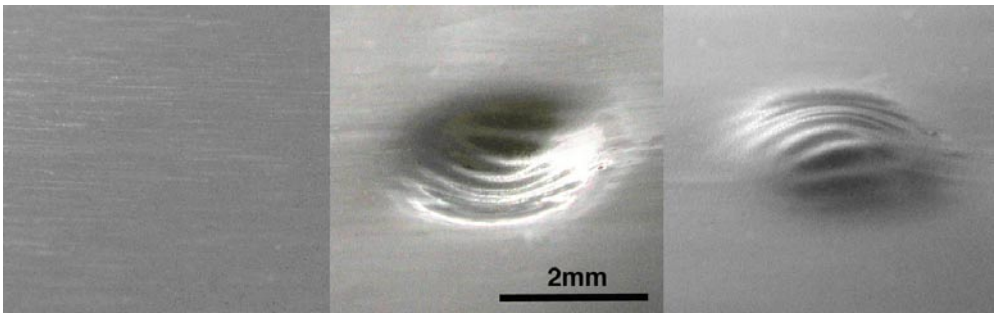

Figure 11. Photographs illustrating deformation in target foils created by the reflected wave field from a parabolic reflector. Foils were exposed to shock waves at overpressure to preclude cavitation (∼12 MPa). The left image is of a foil positioned at F2 with no reflector near it. This foil was treated with 100 shock waves and shows no damage. The other two images show the two sides of a foil that was mounted 3 mm proximal to the parabolic reflector (within the overpressure chamber) and treated with the same dose of shock waves as the foil at the left. Shock wave exposure generated a dent with a wrinkled surface. The central frame shows the side of the foil facing the reflector, the right frame shows the opposite side.

from bubbles or from the reflector, or from a primary collapse event. Again, elevating the overpressure above 5.5 MPa eliminated these emissions.

3.3. Foil damage

When aluminium foils are exposed to lithotripter shocks at atmospheric pressure 'pitting' damage is commonly seen (e.g. Lifshitz *et al* 1997, Bailey *et al* 1999a). These pits have been observed to be of the form of rounded depressions (<1 mm wide) with a toroidal ring surrounding this depression (Coleman *et al* 1987b). Such pitting deformation has been attributed to asymmetrical bubble collapse in the vicinity of the foil. In contrast, foils subjected to the reflected wave field of the parabolic reflector (figure 11) at an overpressure of ∼12 MPa showed completely distinct deformation features. A *single* depression/dent with a wrinkled surface was observed. This dent was ∼4 mm wide which corresponds to the 6 dB region of the refocused wave (5 mm; see table 1). The wrinkling deformation could be described as a series of adjacent peaks and troughs on the foil observed over the dented area. No such denting and wrinkling deformation was seen for foils exposed to the lithotripter wave field either at atmospheric or at elevated pressures. Hence the above deformation features of aluminium foils were due to the refocused wave field from the parabolic reflector and not due to bubble collapse.

3.4. Cell lysis results

Cell lysis experiments were conducted with the vials at >12 MPa overpressure. In previous work we have shown that relatively low overpressure (∼0.3 MPa) eliminates cavitation in water in the free field (Bailey *et al* 1999b). Also we have shown that cell lysis is dramatically reduced, but is not eliminated at overpressures that preclude cavitation (Williams *et al* 1999b). In those experiments, using the same overpressure chamber, cells contained in rigid polypropylene vials were exposed to half the number of shock waves (75) as in the present study; shock wave induced cell lysis at high pressure was $1.03 \pm 0.09\%$ compared with $0.53 \pm 0.02\%$ for untreated controls. In the present study, also at overpressure to preclude cavitation, lysis with the parabolic reflector ($4.2 \pm 0.4\%$) was approximately four-fold higher, and lysis with the

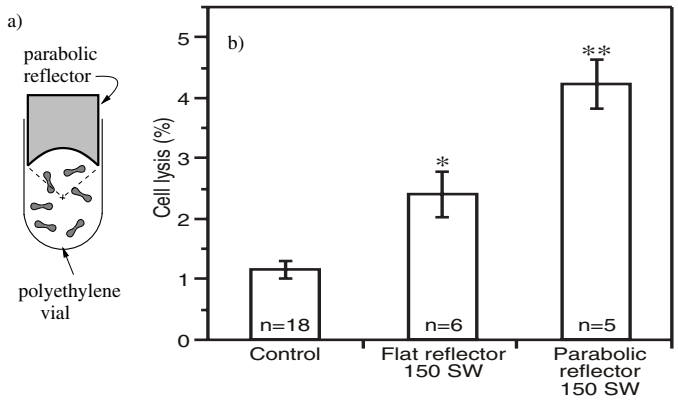

Figure 12. (*a*) Schematic of parabolic reflector inserted into a polyethylene vial containing a suspension of RBCs (cells drawn larger than scale). (*b*) Lysis of RBCs in suspension, in the presence of either the flat or parabolic reflector. 'Control' includes groups controlling for handling and pressurization effects (which were not significant) and received no shock waves. Shock waves were administered at 20 kV and 1 Hz. n indicates number of trials for each case. *Different from control and parabolic, $p < 0.01$; **different from control, $p < 0.001$.

flat reflector ($2.4 \pm 0.4\%$) was about twice that of untreated controls ($1.2 \pm 0.2\%$). Thus, shock-wave induced cell lysis not due to cavitation was significantly enhanced by the reflected wave field.

4. Discussion

Most studies of tissue damage in SWL have focused on cavitation as the damage mechanism (e.g. Delius 1997, Coleman *et al* 1987b). In previous studies (Williams *et al* 1999b) we demonstrated cell lysis due to lithotripter shock waves under conditions in which cavitation was prevented. In that report we suggested that cell lysis in the absence of cavitation may have been due to shear. The notion that shearing motion of fluid causes deformation of cells and subsequently causes them to lyse has been widely accepted in other applications and is also applicable to flow fields induced by SWL shock waves (Howard and Sturtevant 1997). Shear flow induces stress/strain in cell membranes and can result in irreversible leakage of cellular contents. In this work we enhanced this shearing effect by refocusing the lithotripter wave with a parabolic reflector and observed increased cell lysis.

The gradient in shock strength for the wave focused by the parabolic reflector was measured to be twice that of the lithotripter shock wave. As mentioned in the introduction, besides the shock wave gradient, the wavefront curvature also contributes to the flow-field parameter ($k(t)$) which characterizes the deformation rate of the fluid and suspended cells. Since the PVDF hydrophone provides measurement at a single location, wavefront curvature cannot be obtained from this measurement. However, we estimate that the contribution of the curvature effect to $k(t)$ will be of the same order of magnitude (see paper I) as the wavefront gradient. Also, nonlinearity effects cause 'kinks' to form in the shockfront (Sturtevant and Kulkarny 1976) (see also paper I). These 'kinks', if present, would increase the value of $k(t)$ by several orders of magnitude, but these cannot be detected by our current measurement system.

In paper I we analysed stress/strain in a cell membrane when suspended in a general fluid flow-field. The flow-field of a focused shock and the radial motion due to bubble expansion were found to be lytically effective since they were able to induce stresses of the order of

the critical stress required to rupture a RBC membrane. However, the shock wave flow-field applies this stress for a very small duration, and the membrane strain is estimated to be several orders smaller than that required for failure. Hence, the fraction of cells lysed due to lithotripter shock waves under conditions which preclude cavitation was smaller ($\sim$0.5% above control after 75 shocks) (Williams *et al* 1999b) than lysis under atmospheric conditions (1.5–6.5% above control, depending on cell suspension and vial orientation; Williams *et al* 1999b), where cavitation occurs. In this work, the refocused wave field from the parabolic reflector lysed $\sim$3% cells above control after 150 shocks, whereas the reflected wave field from a flat reflector lysed only 1% cells above control. Thus, cell lysis correlated with shock-strength gradient and corroborated the shearing mechanism.

In the present work we devised a novel cavitation detector (HP-PCD) which measured acoustic emission from the focal region of the lithotripter under conditions of high overpressure. The free-field acoustic emission measured by our PCD indicated the typical double-bang signature. The presence of a parabolic or a flat reflector at F2 modified this signal and delayed the collapse of the bubble cloud. However, this signal was conspicuously absent in the presence of the pressure chamber. The influence of the pressure chamber on cloud collapse could be possibly due to one of the following: waves reflecting from the cylinder walls cause the bubble cloud to collapse prematurely; since the chamber restricts free circulation of water, cavitation nuclei are not easily available and hence the lack of cloud formation and collapse. An overpressure of 5.5 MPa was determined to be sufficient to suppress all acoustic emission.

Aluminium foil targets were exposed to the lithotripter wave field and the reflected wave field at various overpressures. Aluminium foils subjected to the refocused wave at an overpressure $\sim$12 MPa did not show the typical pitting damage, but instead a single depression/dent with wrinkled surface was observed. Unlike pitting damage which can be suppressed by applying overpressure, these deformation features were persistent at elevated pressures. The dent formed on the foil can be obtained by the application of a force which is concentrated at the centre of the foil and reduces radially outwards. Such a force distribution is consistent with the off-axis distribution of peak pressures of the refocused wave field and the dent dimension corresponds to the 6 dB width of the refocused wave field. Hence, these foil deformation features are attributed to the refocused shock wave.

In conclusion, cell lysis results clearly indicate increased cell damage due to the refocused shock wave from the parabolic reflector. The results are in qualitative agreement with the prediction in paper I that a refocused shock wave has a higher cell lysis because of the higher deformation parameter $k(t)$, as compared with the lithotripter wave. Theory is as yet unable to predict the fraction of lysed cells, thus, a direct comparison with our experimental result must await such a development. However, these results validate the hypothesis of shear-induced cell lysis due to a differential in shock strength, and improve our understanding of the physical mechanisms responsible for tissue injury in SWL.

Acknowledgments

We thank Dr Michael Bailey of Applied Physics Laboratory, University of Washington, for providing the PVDF membrane hydrophone and Dr Robin Cleveland of Boston University for his assistance with the design of HP-PCD. We also thank Dr Lawrence Crum and Dr Tim Colonius for their comments and suggestions. This work was supported by NIH Grant P01 DK43881.

References

Bailey M R, Blackstock D T, Cleveland R O and Crum L A 1999a Comparison of electrohydraulic lithotripters with rigid and pressure-release ellipsoidal reflectors: II. Cavitation fields *J. Acoust. Soc. Am.* **106** 1149–60

Bailey M R, Cleveland R O, Sapozhnikov O A, McAteer J A, Williams J C Jr and Crum L A 1999b Effect of increased ambient pressure on lithotripsy-induced cavitation in bulk fluid and at solid surfaces *J. Acoust. Soc. Am.* **105** 1267

Choi M J, Coleman A J and Saunders J E 1993 The influence of fluid properties and pulse amplitude on bubble dynamics in the field of a shock-wave lithotripter *Phys. Med. Biol.* **38** 1561–73

Church C C 1989 A theoretical study of cavitation generated by an extracorporeal shockwave lithotripter *J. Acoust. Soc. Am.* **86** 215–27

Cleveland R O, Bailey M, Fineberg N, Hartenbaum B, Lokhandwalla M, McAteer J A and Sturtevant B 2000b Design and characterisation of a research electrohydraulic lithotripter patterned after the Dornier HM3 *Rev. Sci. Instrum.* **71** 2514–25

Cleveland R O, Sapozhnikov O A, Bailey R M and Crum L A 2000a A dual passive cavitation detector for localized detection of lithotripsy-induced cavitation *in vitro J. Acoust. Soc. Am.* **107** 1745–58

Coleman A J, Choi M J, Saunders J E and Leighton T G 1992 Acoustic emission and sonoluminescence due to cavitation at the beam focus of an electrohydraulic shock wave lithotripter *Ultrasound Med. Biol.* **18** 267–81

Coleman A J, Saunders J E, Crum L A and Dyson M 1987b Acoustic cavitation generated by an extracorporeal shock wave lithotripter *Ultrasound Med. Biol.* **13** 69–76

Coleman A J, Saunders J E, Preston R C and Bacon D R 1987a Pressure wave-forms generated by a Dornier Extracorporeal Shockwave Lithotripter *Ultrasound Med. Biol.* **13** 651–7

Delius M 1997 Minimal static pressure minimizes the effect of extracorporeal shock waves on cells and reduces it on gallstones. *Ultrasound Med. Biol.* **23** 611–17

Dunn F 1985 Cellular activation by heat and shear *Radiat. Environ. Biophys.* **24** 131–9

Eisenmenger W, Köhler M, Pech R and Wurster C 1997 Negative pressure amplitudes in water measured with fiber optic hydrophone *Prog. Nat. Sci.* **7** 499–501

Evan A P and McAteer J A 1996 Q-effects of shock wave lithotripsy *Kidney Stones: Medical and Surgical Management* ed F L Coe and M J Favus (Philadelphia, PA: Lippincott-Raven) 549–70

Evans E A, Waugh R and Melnik L 1976 Elastic area compressibility modulus of red cell membrane *Biophys. J.* **16** 585–95

Howard D D and Sturtevant B 1997 *In vitro* study of the mechanical effects of shock wave lithotripsy *Ultrasound Med. Biol.* **23** 1107–22

Kaude J V, Williams C M, Millnder M R, Scott K N and Finlayson B 1985 Renal morphology and function immediately after extracorporeal shock-wave lithotripsy *Am. J. Roentgenol* **145** 305–13

Leverett L B, Hellums J D, Alfrey C P and Lynch E C 1972 Red blood cell damage by shear stress *Biophys. J.* **12** 257–73

Lifshitz D A, Williams J C Jr, Sturtevant B, Connors B A, Evans A P and McAteer J A 1997 Quantization of shock wave cavitation damage *in vitro Ultrasound Med. Biol.* **23** 461–71

Lokhandwalla M and Sturtevant B 2001 Mechanical haemolysis in ESWL I: Analysis of cell deformation due to ESWL flow-fields *Phys. Med. Biol.* **46** 413–37

Müller M 1990 Comparison of Dornier lithotripters: measurement of shock wave fields and fragmentation effectiveness *Biomed. Tech.* **35** 250–62

O'Niel H T 1949 Theory of focusing radiators *J. Acoust. Soc. Am.* **21** 516–26

Rayleigh J W 1917 On the pressure developed in a liquid during the collapse of a spherical cavity *Phil. Mag.* **34** 94–8

Rooney J A 1970 Hemolysis near an ultrasonically pulsating gas bubble *Science* **169** 869–71

——1972 Shear as a mechanism for sonically induced biological effects *J. Acoust. Soc. Am.* **52** 1718–24

Saas W, Braunlich M, Dreyer H P, Matura E, Folberth W, Priesmeyer H G and Siefert J 1991 The mechanisms of stone disintegration by shock waves *Ultrasound Med. Biol.* **17** 239-43

Stonehill M A, Williams J C, Bailey M R, Lounsbery D, Cleveland R O, Crum L A, Evan A P and McAteer J A 1998 An acoustically matched high pressure chamber for control of cavitation in shockwave lithotripsy: mechanisms of shock wave damage *in vitro Methods Cell Sci.* **19** 303–11

Sturtevant B 1996 Shock wave physics of lithotripters *Smith's Textbook of Endourology* ed A D Smith (St Louis, MO: Quality Medical) pp 529–52

Sturtevant B and Kulkarny V A 1976 The focusing of weak shock waves *J. Fluid Mech.* **73** 651–71

Vogel A and Lauterborn W 1988 Acoustic transient generation by laser-produced cavitation bubbles near solid boundaries *J. Acoust. Soc. Am.* **84** 719–31

Williams J C, Stonehill M A, Colmenares K, Evan A P, Andreoli S P, Cleveland R O, Bailey M R, Crum L A and McAteer J A 1999a Effect of macroscopic air bubbles on cell lysis by shock wave lithotripsy *in vitro Ultrasound Med. Biol.* **25** 473–9

Williams J C, Woodward J F, Stonehill M A, Evan A P and McAteer J A 1999b Cell damage by lithotripter shock waves at high pressure to preclude cavitation *Ultrasound Med. Biol.* **25** 1445–9

Zhong P, Cioanta I, Cocks F H and Preminger G M 1997 Inertial cavitation and acoustic emission produced during electrohydraulic shock wave lithotripsy *J. Acoust. Soc. Am.* **101** 2940–50

Zhong P, Xi X F, Zhu S L, Cocks F H and Preminger G M 1999 Recent developments in SWL physics research *J. Endourol.* **13** 611–17